Seismic health monitoring of an instrumented multistory building using the interpolation method

M. P. Limongelli*,†

Department of Architecture, Built Environment and Construction Engineering, Politecnico di Milano Piazza Leonardo da Vinci 32, 20133 Milano, Italy

Received 15 March 2013; Revised 25 November 2013; Accepted 14 January 2014

1. INTRODUCTION

Seismic structural monitoring is an important tool for both rapid post-event assessment and also for a prompt detection of damage before the structure reaches a critical state. Traditional methods of damage detection based on walk-through visual inspections or experimental techniques such as radiography or ultrasound allow to obtain detailed information about a local damage state but require that the vicinity of damage is already known and easily accessible. These techniques may be costly, taking a long time to be performed and impractical to detect damage in large urban areas. Furthermore, they may fail if damage is not visibly evident.

A promising alternative able to provide information on the structural health consists in the use of responses recorded by digital accelerometers commonly installed in instrumented buildings. On the basis of these responses and applying an appropriate damage detection technique, a quick assessment of the damage state of the building after a seismic event can be obtained. In the last 20 years, several approaches have been proposed for damage identification based on the analysis of responses to vibrations recorded on the structures. One of the most important aspects of these 'vibration-based damage detection technique' is the definition of a damage-sensitive feature able to reliably assess damage and easily recoverable from the building responses without heavy computational work. From a practical point of view, the latter aspect is particularly important because it allows to reduce the pre-earthquake investments that the owners may not be willing to sustain, needed to characterize the original (undamaged) state of the building [1].

*Correspondence to: M. P. Limongelli, Department of Architecture, Built Environment and Construction Engineering, Politecnico di Milano, Piazza Leonardo da Vinci 32, 20133 Milano, Italy.

†E-mail: limongelli@stru.polimi.it

Great part of the methods proposed in literature carry out the identification of damage through comparison of the undamaged state of the system with the damaged one. The different ways to carry out this comparison have led to a number of different approaches: References [2–4] give complete bibliographic reviews.

A number of methods are based on the updating of a numerical model of the structure carried out modifying the values of certain structural parameters more sensitive to damage so that the calculated responses of the model match the ones recorded on the damaged structure. The problem of damage detection is tackled as an optimization problem where the values of the damage parameters are sought as the ones that minimize a certain objective function [5]. The main drawback of this family of methods is the need of an accurate three-dimensional (3D) numerical model that, for the great part of structures, has a large computational demand and can be difficult to build. Furthermore, the updating of the model usually requires some time; hence, it is performed 'offline', slowing down the process of damage detection.

The same drawback, coming out from the need of a detailed numerical model, affects neural network approaches [6, 7]. These latter consist in 'training a neural network' of the structure by the data obtained from the undamaged system and then feed the trained system and the real structure with the same input. The difference (error) between the outputs of the real system and of the network is a measure of the damage to the structure. This kind of methods require large sets of data from different damage scenarios in order to train the network, and because for the majority of the structures these data are not available, the networks have to be trained using numerical models of the building that have to be very detailed.

A different and very diffuse approach to the problem of damage detection is based on the analysis of changes of modal characteristics between the original (undamaged) state and the (possibly damaged) current state [8–15]. Methods based on frequency changes can be reliably applied to detect damage, but they are hardly able to give information about the location of damage. To this aim are more effective methods based on the analysis of changes of modal shapes or of their derivatives. Several researches however have pointed out that modal parameters alone are not robust estimators of damage being sensitive to errors introduced by the experimental process needed for their evaluation and to environmental changes (temperature, moisture, loading condition), to nonlinearity in the building response or soil–structure interaction and to noise in recorded data [16].

To overcome some of these problems, nonmodal methods that do not need the estimation of modal parameters have been proposed. Some are based on the use of frequency response functions (FRFs) as damage-sensitive parameter [17–19]; others as the frequency response curvature method and the gapped smoothing method proposed in References [20, 21], both define the damage index in terms of the variation of curvature estimated from operational deformed shapes recovered from FRFs. The main advantage of the nonmodal approach to the problem of damage detection, beyond the fact that modal analysis becomes unnecessary, is that FRFs and the corresponding deformed shapes and curvatures, being defined on the whole frequency range, contain broadband data. This is hardly achieved using modal shapes because current procedures of modal parameters extraction are usually effective only for a limited number of lower modes; hence, information relevant to the higher frequency range are often lost. Furthermore, FRFs, if calculated in terms of acceleration, can be recovered directly from the time histories of recorded signals without resorting to displacements that are sometimes tricky to evaluate from recorded accelerations.

The main drawback of both frequency response curvature method and gapped smoothing method is that the numerical differentiation needed to evaluate curvature from operational deformed shapes introduces errors that often prevent the detection of damage in case of noisy data.

The interpolation damage detecting method (IDDM) recently proposed by the author [22, 24] reduces errors related to differentiation through the definition of the damage index based on operational deformed shapes rather than curvatures. The damage feature is the interpolation error related to the use of a spline function in modeling the operational deformed shapes of the structure: Statistically significant variations of the interpolation error between two successive inspections of the structure indicate the onset of damage. The IDDM has been successfully applied to bridges [22, 23], to plane frames [24] and, in its 2D formulation, to plates [25].

In order to avoid false or missing indications of damage related to random variations of the damage feature not related to damage, their effect should be properly taken into account. In a previous paper

[24], the author proposed a statistical framework based on hypothesis testing aimed to detect significant variations of the damage index, neglecting those due to random fluctuations. This approach is based on the knowledge of the statistical distributions of the damage feature in the original configuration. For the example presented in Reference [24], the statistical distribution of the interpolation error was estimated at each location by making 1000 copies of the FRF corresponding to the undamaged configuration and corrupting each copy with a different Gaussian noise vector. A more realistic application of the statistical procedure requires the availability of several sets of responses recorded on a structure.

The focus of this paper is on the application of the IDDM to a real instrumented 3D structure, more complex that a plane frame, using responses recorded by a permanent network of accelerometers. To this aim, the factor building, a densely instrumented building at the University of California, Los Angeles (UCLA) campus, has been considered. After Northridge earthquake in 1994, the building was instrumented by the US Geological Survey with 72 channels of acceleration sensors and several small to medium earthquakes have been recorded by the array [28]. Responses recorded on the real building have been used to study the statistical variability of the interpolation error and to calibrate a numerical model of the building. At the time being, only responses recorded during events that did not damage the factor building are available; hence, it is not possible to test the performance of the IDDM using real recorded responses. To this aim, a numerical model of the building was developed, calibrated using responses recorded on the structure, and used to simulate several different damage scenarios in order to check the performance of the IDDM.

2. METHODOLOGY

2.1. The basic idea

The idea underlying the IDDM can be schematically explained with reference to Figure 1. The two pictures show a snapshot of the deformed shape of two multistory shear frames undergoing a seismic excitation. The only difference between the two frames is the value of the stiffness of the fifth story columns that, in the frame on the right, is equal to the 80% of the corresponding value in the left frame. Such a reduction of stiffness is assumed to model a damage concentrated at the fifth story.

The comparison of the two pictures shows that damage causes a sharp variation of the deformed shape occurring at the damaged story. In the stories located below and above the damaged one, the two shapes can be almost perfectly superimposed with a simple horizontal shift in the region above the damaged story.

A damage detecting feature can thus be defined in terms of the error related to the use of a certain function in modeling the deformed configuration of the structure. Specifically, at a given location of a structure, the interpolation accuracy can be defined as the difference between the measured displacement and the displacement calculated at that location by interpolating, through a proper

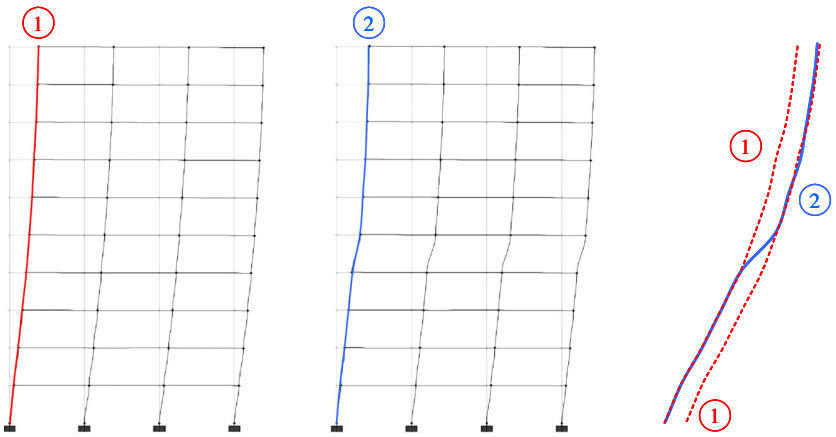

Figure 1. Effect of damage.

function, the displacements measured at all the other locations equipped with a sensor. If the comparison between the interpolation error in two different phases (the baseline phase on the undamaged structure and the inspection phase after a potentially damaging event) highlights a significant decrease of accuracy, this is an indication of the existence of damage at a location close to the one where this change has been recorded.

2.2. *The damage localization procedure*

In order to remove the influence of the amplitude of displacement on the evaluation of the error function and to remove the errors related to the estimation of displacements from recorded accelerations, the error function has been defined in terms of difference between the transfer functions of the recorded and interpolated accelerations with respect to the input acceleration.

Let z_0, z_1,…, z_n, be the instrumented location of the structure where responses in terms of acceleration have been recorded.

The FRF at each location z can be calculated interpolating through a spline shape function the FRFs calculated form signals recorded at all the other instrumented locations (the dotted line in Figure 2).

At the lth location z_l the FRF can be calculated through the spline interpolation using the following relationship:

$$H_s(z_l,f_i) = \sum_{j=0}^{3} c_{j,l}(f_i)\left(z_l - z_{l-1}\right)^j \qquad z\in\left[z_{l-1} - z_l\right], \tag{1}$$

where the coefficients (c_{0l}, c_{1l} c_{2l} c_{3l}) are calculated from the values of the transfer functions 'recorded' at the other locations:

$$c_{j,l}(f_i) = g(H_R(z_k,f_i)) \qquad k\neq l \tag{2}$$

The explicit expressions of the coefficient of the spline function $c_{j,l}$ in terms of the FRF's are determined imposing continuity of the spline function and of its first and second derivative in the knots (that is at the ends of each subinterval). More details on the spline interpolation procedure to calculate acceleration responses can be found in Reference [26].

In terms of FRF's, the interpolation error at location z (in the following the index l will be dropped for clarity of notation) at the ith frequency value f_i, is defined as the difference between the magnitudes of recorded and interpolated FRFs:

$$E(z,f_i) = |H_R(z,f_i) - H_S(z,f_i)| \tag{3}$$

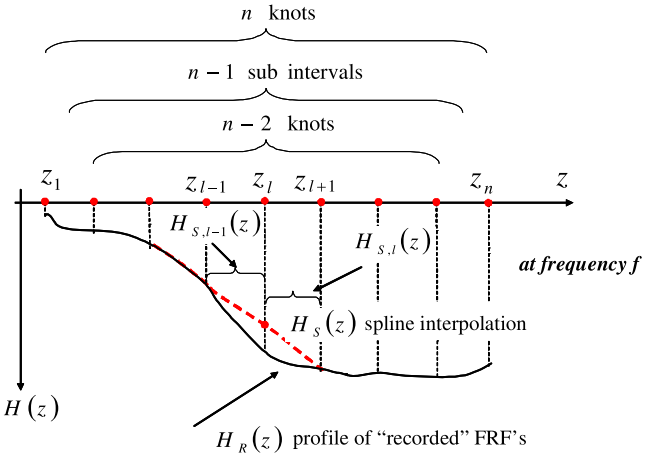

Figure 2. Spline interpolation of the frequency response function at $z = z_l$.

where H_R is the FRF of the response recorded at location z and H_S is the spline interpolation of the FRF at z. In order to characterize each location with a single error parameter, the norm of the error on the whole range of frequencies has been considered:

$$E(z) = \sqrt{\sum_{i=n_o}^{n_o+N} E(z,f_i)^2} \tag{4}$$

N is the number of frequency lines in the Fourier transform correspondent to the frequency range starting at line n_o, where the signal-to-noise ratio is high enough to allow a correct definition of the FRF.

The values of the FRFs depend on the state of the structure; hence, if the estimation of the error function through Equation (4) is repeated in the baseline (undamaged) and in the inspection (potentially damaged) phases, the comparison between the two values E_0 and E_i, respectively, should give an indication about the existence of damage at the considered location.

$$\Delta E(z) = E_i(z) - E_o(z) \tag{5}$$

An increase in the interpolation error at a station between the reference configuration and the current configuration highlights a localized variation in the operational deformed shape and therefore a local variation of stiffness, associated with damage.

2.2.1. Statistical variability of the interpolation error. Several sources, such as temperature, moisture, nonlinear behavior, soil–structure interaction, noise in recorded data, and excitation sources, can induce variations of the interpolation error even if no damage occurs. To take into account the effect of these random variations in the damage localization procedure, the statistical variability of the interpolation error E in the undamaged configuration should be investigated in order to extract the relevant probability distribution $f_{E,0}$ at each instrumented location z.

In Figure 3, the distribution in the undamaged configuration $f_{E,0}$ at one location z is compared with the distribution in the damaged state $f_{E,d}$; damage close to location z induces an increase of the interpolation error at z hence a shift of the distribution toward higher values.

If the two distributions $f_{E,0}$ and $f_{E,d}$ or their estimates were known, the onset of damage at a given location z could be investigated by checking the variations of the mean value of the distribution in the inspection phase μ_I with respect to the original phase μ_0. Usually, while $f_{E,0}$ can be estimated on the basis of a large sample of values of E_0 calculated from responses recorded on the undamaged (original) structure, in the inspection phase, only one value of E_I is available; hence, the distribution $f_{E,I}$ and its parameters cannot be estimated. At each instrumented location z of the structure the value of the interpolation error $E_I(z)$ in the 'inspection' configuration has to be compared with the distribution in the undamaged configuration to check if and where (at which location) there has been a significant increase of the interpolation error.

If any change of this parameter is assumed as a proof of damage, a large number of *false alarms*, namely to consider as erroneously damaged sections that are actually intact, arise. This is certainly

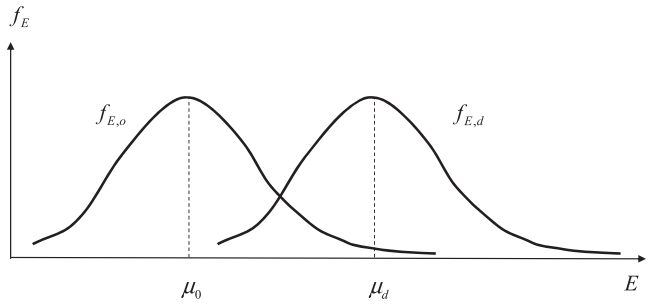

Figure 3. Distributions in the undamaged ($f_{E,0}$) and in the damaged ($f_{E,d}$) configurations.

on the safe side from the security point of view but can lead to (expensive) unnecessary alarms about the structural condition.

In order to distinguish a *significant* increase of E, a threshold value can be defined so that if the variation is over the threshold, the location is assumed as damaged; otherwise, the variation is assumed to be due to random sources.

The threshold E_T can be defined as the value of the interpolation error beyond which the probability that the structure is undamaged is 'sufficiently' low; hence, it is worth to give an alarm about the structural condition.

Of course, even if the value of the interpolation error E_I is higher than the threshold E_T, there is still a (low) probability, represented by the squared area P_f in Figure 4, that the structure is undamaged. In this case, being the value of the interpolation error in the inspection phase E_I beyond the threshold, an alarm is given, but it is a false alarm because the structure is undamaged. The probability of false alarm P_f corresponding to the value E_T of the threshold is given by:

$$P_f = P[E_I > E_T | no\ damage] \tag{6}$$

Somehow, this probability represents the *owner risk* that is the probability that for an integer building, an unnecessary (but costly) intervention is required to the owner of the building.

In addition to the probability of false alarm, the value E_T of the threshold defines a value of the *probability of missing alarm* P_m that is the probability that the variation of the interpolation error is mistakenly attributed to random sources while it is actually due to damage. If the structure is damaged but the value E_I is lower than the threshold, no alarm is given. In this case, there is a *missing alarm* because the structure is actually damaged. The probability of missing alarm, represented by the hatched area P_m, under the $f_{E,I}$ in Figure 4 is given by:

$$P_m = P[E_I < E_T | there\ is\ damage] \tag{7}$$

and can be considered as the *user risk* that is the probability that for a damaged building, the necessary intervention is not carried out, thus jeopardizing the lives of the building's users.

The definition of the threshold is thus a trade-off between the probability of false and missing alarm that is between the user's and the owner's risk, and it must be the object of preliminary analysis based on the consequences of the two types of error: If a false alarm is considered too expensive, then a high value of the threshold is appropriate. On the contrary, if the consequences of a false alarm are not really a problem while the consequences of a missing alarm can be very serious, then case a low value of the threshold should be chosen. The choice of the threshold basing on a cost–benefit analysis is beyond the scope of this paper and will not be performed for the application reported in the following. The threshold E_T will be fixed on the basis of a given value of the tolerable probability of false alarm P_f that is basing on the tolerable owner's risk. A (theoretical) alternative could have been the estimation of the threshold basing on the accepted user risk that is the probability of missing alarms. Actually, while P_f depends on the distribution of E_0, the interpolation error in the undamaged state,

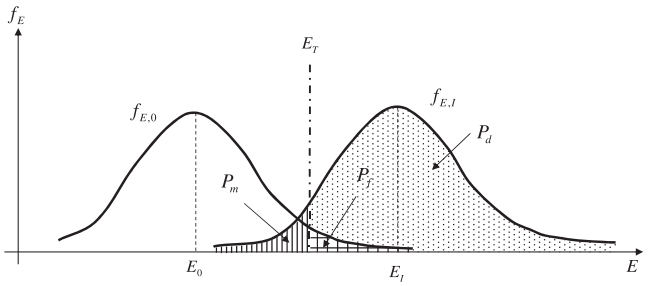

Figure 4. Distribution of the interpolation error in the undamaged $f_{\mu,0}$ and in the inspection $f_{\mu,I}$ configurations.

P_m depends on the distribution of E_I, the interpolation error in the inspection state. This second distribution is usually unknown before the occurrence of damage, and this is the reason why the reference herein made to P_f instead of P_m.

The threshold E_T is thus defined as the (1-P_f)th percentile of the cumulative distribution F_{Eo} of the interpolation error E_o in the undamaged configuration. At a given location z, the value of the threshold $E_T(z)$ is defined by the following relationship:

$$F_{Eo}(E_T(z)) = 1 - P_f \tag{8}$$

Once the threshold is known, the interpolation damage index (IDI) can be calculated at location z as the positive difference between the actual value of the interpolation error and the threshold:

$$\begin{aligned} IDI(z) &= E(z) - E_T(z) \qquad if \qquad E(z) \geqslant E_T(z) \\ IDI(z) &= 0 \qquad\qquad\quad if \qquad E(z) < E_T(z) \end{aligned} \tag{9}$$

It must be noted that at different locations different values of the thresholds will be calculated for the same probability of false alarm P_f.

The exceedance of the value of the threshold E_T can give a measure of the severity of damage at that location. This difference can thus be used to establish a hierarchy between damaged locations and to draw up a priority list between damaged locations for both immediate interventions and of future strengthening intervention.

The application of the IDI contemplates two phase:In the undamaged phase:

(1) Estimation of the distribution of the interpolation error $E_o(z)$ in the undamaged configuration at each instrumented location z.
(2) Computation of the value of the threshold $E_T(z)$ basing on value chosen for the tolerable risk of false alarm P_f.

In the inspection phase:

(3) Computation of the current value of the interpolation error $E_I(z)$ at each instrumented location z.
(4) Checking of the structural health at each instrumented location z through the comparison between $E_I(z)$ and $E_I(z)$ using Equation (9).

2.3. Description of the building and of the sets of responses

In this paper, the IDDM has been tested using signals recorded on a real building densely instrumented and for which responses recorded during several earthquakes are available.

The choice of the factor building has been carried out for two main reasons. The factor building is one of the few examples of a densely instrumented building, suitable for the application of the IDDM algorithm whose accuracy increases with the density of recording sensors.

Because of this diffuse network of recording sensors and the consequent availability of a large set of real data recorded on this building, it was possible to study the statistical variation of the damage feature (interpolation error) in the undamaged configuration based on real recorded data and not on a numerical simulation.

Because the factor building has not suffered permanent damages after the installation of the current network of sensors, in order to check the damage localization algorithm, a numerical model of the building was used. The application to this model allowed the simulation of the responses of a real 3D building in a damaged configuration, hence a more reliable check of IDDM.

The UCLA factor building (Figure 5) is a 17-story moment-resisting steel frame structure consisting of two stories below grade and 15 above grade. The building houses laboratories, faculty offices, administrative offices, the School of Nursing, School of Medicine, auditoriums, and classrooms.

The building plan is approximately rectangular, longer in the north-south (u, x) direction and fairly symmetric about the east-west (y) axis. The lateral resisting system is a double-bay moment frame with

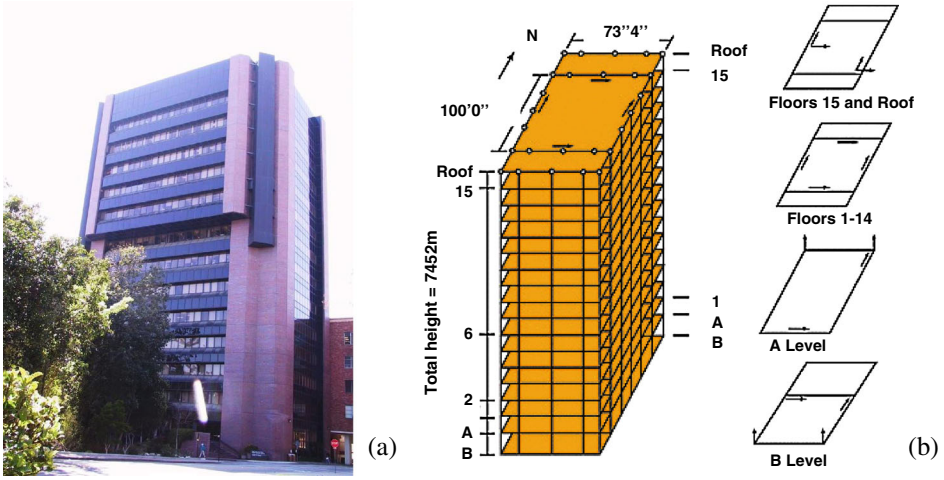

Figure 5. The factor building (a) east face; (b) sensors location (from Reference [28]).

fixed connection between beams and columns. A gravity frame with pinned beams completes the structural scheme. The floors consist of lightweight concrete slab on metal decking. The façade is made of Norman face brick veneer (BV) and glass curtain walls (GCWs) supported by an aluminum frame.

The building is permanently instrumented with an embedded 72-channel accelerometer array recording both ambient vibrations of the building and motions from local earthquakes. The sensors array is composed by four horizontal channels per floor: two in the north-south direction and two in the east-west direction. The two floors below grade are also equipped with two vertical channels. The array continuously records ambient vibrations and motions from local earthquakes. More details on the factor building and on the recording network can be found in References [28, 30].

The network of sensors deployed on the factor building records responses in two directions as showed in Figure 5(b): At each floor, four responses are recorded, two in the north directions located in the east (NE) and in the west (NW) part of the building and 2 in the east direction in the north (EN) and in the south (ES) part of the building (Figure 6).

Assuming a rigid diaphragm behavior of each floor, the four recorded responses have been used to calculate the two components of the absolute accelerations in x and y directions at the reference point R (Figure 6).

The following relations were used to calculate floor accelerations:

$$\begin{aligned} \ddot{\theta}_R &= \frac{1}{2}\left[\frac{(\ddot{u}_2 - \ddot{u}_1)}{(y_1 + y_2)} + \frac{(\ddot{v}_2 - \ddot{v}_1)}{(x_1 + x_2)}\right] \\ \ddot{u}_R &= \ddot{u}_1 + \ddot{\theta}_R y_1 \\ \ddot{v}_R &= \ddot{v}_1 + \ddot{\theta}_R x_1 \end{aligned} \tag{10}$$

2.4. *Statistical analysis of the interpolation error in the 'undamaged state' of the factor building*

Different research groups have studied responses recorded on the factor building during ambient vibrations of during small earthquakes detecting small variations in vibration characteristics. In Reference [31], the authors report the detection of temporal changes of the vibration characteristics during small earthquakes (Yorba Linda and Encino): The 'pre-earthquake' characteristic is recovered after a very small period (from some minutes to some hours). In the first case, the changes of the modal characteristics are attributed to 'soil–structure interaction' (no damage to the structure), in the second case to 'increased amplitudes due to a combination of the Encino earthquake and strong winds' (no damage to the structure).

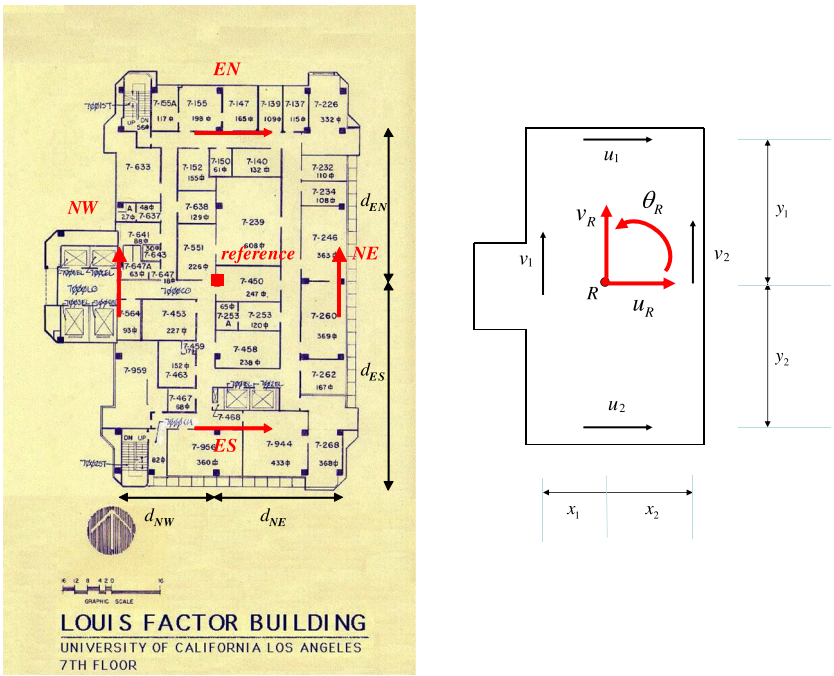

Figure 6. Floor plan: sensors location and reference point on the floor [28].

In Reference [27], on the basis of the analysis of responses recorded during ambient vibrations, the authors show that modal frequencies and damping exhibit variations up to 7% due to environmental sources, mainly temperature changes, that follow a normal distribution.

No permanent damage was reported on the factor building during the monitoring period; hence, the responses recorded on the building can be reliably used to assess the statistical variation, because of sources other than damage, of parameters related to a reference configuration of the structure.

The availability of responses recorded during a relatively long period allows to carry out a statistical analysis of the interpolation error, the damage feature considered in this paper, in the original (reference) configuration.

The analysis of the variation of the interpolation error on the factor building has been carried out with reference responses recorded during 35 small earthquake occurred throughout 2004 and described in Table I.

Some set of responses recorded during 2004 were discarded because too noisy (earthquakes 20a and 20b) or because incomplete. For example, all sets of responses recorded between June and July 2004 lack responses at the first and second story. The acceleration time histories, each 30,000 points long (about 5 min at 100 Hz sampling), were downsampled at 50 Hz in order to remove high frequency noise and to reduce the size of data. Signals were then detrended and band-pass filtered in the range 0. 5–8 Hz in order to have a cut-off frequency outside the range of the fundamental modal frequencies of the frame.

For each set of responses the interpolation error $E(z)$ in Equation (4) was calculated at each instrumented location z following the procedure described in Section 2.2 for the two directions x and y. The estimation of $E(z)$ in Equation (4) was carried out assuming $n_o = 30$ and $N = 400$ corresponding to the frequency range between 0.35 Hz and 5.2 Hz.

Figure 7 shows the variation along the height of the building of functions $E_{ox}(z)$ and $E_{oy}(z)$ calculated from responses recorded during the small earthquakes described in Table I.

The values of E_{ox} and E_{oy} exhibit variations at each location even if no damages have been detected on the structure during this period. As previously recalled, these variations are due to several causes such as measurement errors, excitation sources, or variation of environmental conditions (temperature, humidity, soil) that temporarily modify the structural characteristics; hence, the FRFs basing on which the interpolation errors are calculated.

Table I. Sets of responses used for the statistical analysis.

Id	Date	Magnitude	Distance (km)	Descriptive location
45	14 February 2004	ML = 4.3	125.0	17 km WNW of Wheeler Ridge, CA, USA
48	17 February 2004	ML = 3.4	125.5	16 km WNW of Wheeler Ridge, CA, USA
52a	21 February 2004 (3:39 UTC)	ML = 2.7	18.4	1 km S of El Segundo, CA, USA
52b	21 February 2004 (5:16 UTC)	ML = 2.6	18.8	2 km SSW of El Segundo, CA, USA
77	17 March 2004	ML = 4.5	320.5	
79	19 March 2004	ML = 3.5	141.6	8 km NNW of town of Big Bear Lake, CA, USA
83	23 March 2004	ML = 2.8	12.7	2 km ENE of Los Angeles Airport, CA, USA
88	28 March 2004	ML = 3.8	235.8	18 km SW of Olancha, CA, USA
96	5 April 2004	ML = 3.3	109.0	1 km WNW of Loma Linda, CA, USA
99	8 April 2004	ML = 2.9	25.8	13 km WSW of Manhattan Beach, CA, USA
111	20 April 2004	ML = 3.1	57.1	18 km SSW of Pt. Fermin, San Pedro, CA, USA
121	30 April 2004	ML = 3.2	23.9	7 km S of Malibu, CA, USA
130	9 May 2004	ML = 4.4	150.1	16 km W of Isla Vista, CA, USA
132	11 May 2004	ML = 3.2	60.0	31 km SSW of Pt. Dume, CA, USA
143	22 May 2004	ML = 2.6	32.5	3 km NW of Bellflower, CA, USA
243	30 August 2004	ML = 3.2	80.4	9 km NW of Wrightwood, CA, USA
258	14 September 2004	ML = 3.1	230.2	9 km ENE of Coso Junction, CA, USA
260	16 September 2004	ML = 3.6	188.3	4 km E of Yucca Valley, CA, USA
272a	28 September 2004 (17:15 UTC)	ML = 6.0	262.3	Parkfield, CA area, USA
272b	28 September 2004 (17:24 UTC)	ML = 4.9	259.9	Parkfield, CA area, USA
273a	29 September 2004 (17:10 UTC)	ML = 5.0	276.1	Parkfield, CA area, USA
273b	29 September 2004 (22:54 UTC)	ML = 5.0	147.7	28 km NE of Arvin, CA, USA
274	30 September 2004	ML = 4.9	279.9	Parkfield, CA area, USA
283	9 October 2004	ML = 3.1	85.1	19 km N of Elizabeth Lake, CA, USA
290	16 October 2004	ML = 3.3	75.6	12 km E of Ojai, CA, USA
301	27 October 2004	ML = 3.8	143.8	11 km NW of Big Bear City, CA, USA
304	30 October 2004	ML = 2.7	6.7	2 km ENE of West Hollywood, CA, USA
314	9 November 2004	ML = 3.6	176.7	19 km NNE of Barstow, CA, USA
318	13 November 2004	ML = 4.2	150.6	10 km N of Big Bear City, CA, USA
319	14 November 2004	ML = 3.0	92.7	7 km SW of Devore, CA, USA
329	24 November 2004	ML = 2.5	38.3	9 km NNE of Simi Valley, CA, USA
334	29 November 2004	ML = 4.6	285.6	Parkfield, CA area, USA
347	12 December 2004	ML = 3.7	135.0	12 km SSW of town of Big Bear Lake, CA, USA
351	16 December 2004	ML = 3.6	34.8	16 km SSE of Pt. Dume, CA, USA
354	19 December 2004	ML = 2.6	34.7	16 km SSE of Pt. Dume, CA, USA

In order to assess the variability of the interpolation error E, statistical averaging of the available data is performed to extract the distribution at each story and in each of the two directions x and y. Using the values of the interpolation error calculated for the 35 earthquakes in Table I, the histograms of E_0 have been obtained at each instrumented location in each direction (x and y). Being E defined by Equation (4), it takes only positive real values; hence, a lognormal distribution has been considered to fit the available data.

Figures 8 and 9 show the histograms and the lognormal PDFs of the interpolation error E_0 in x and y directions at a number of stories of the building.

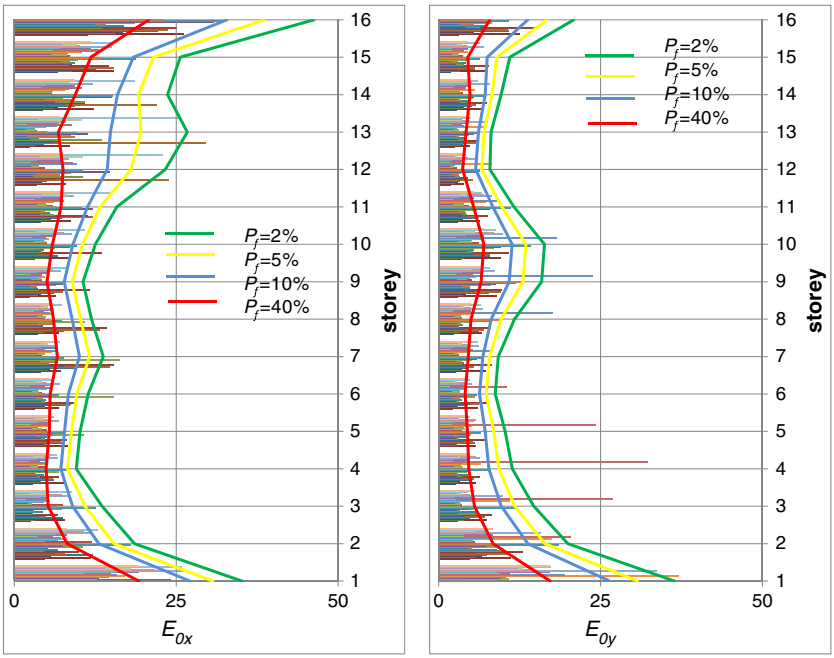

Figure 7. Interpolation errors E_{ox} and E_{oy} and thresholds corresponding to values of the accepted probability of false alarm between 2% and 40%.

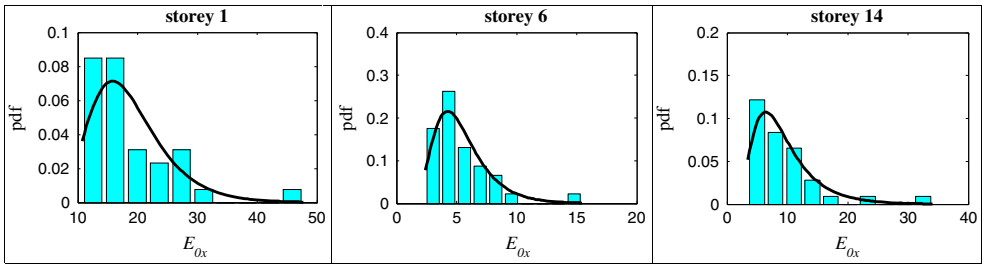

Figure 8. Probability densities of the interpolation error E_{ox} at the 1st, 6th, and 14th stories.

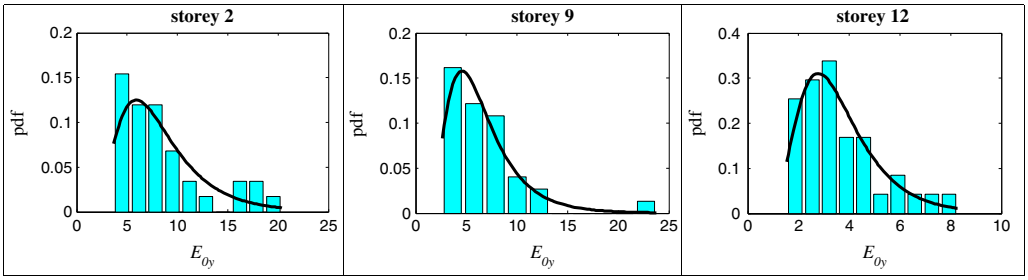

Figure 9. Probability densities of the interpolation error E_{oy} at the 2nd, 9th, and 12th stories.

The parameters of each PDF are estimated using the relevant histogram. The comparison of the histograms and the corresponding PDFs shows that lognormal represents quite correctly the statistical variation of the interpolation error E_0 in the undamaged configuration of the factor building. On the basis of this, the threshold $E_T(z)$ for the definition of the IDI can be calculated at each story z from the value of the inverse cumulative distribution function Φ_z of the lognormal PDF

at that story. The value of the threshold is defined by Equation (8) where P_f is the tolerable value of the probability of false alarm. In Figure 7(a) and (b) are reported, for the directions x and y, the values of the thresholds at each location for different values of P_f: The higher P_f, the lower the value of the interpolation error over which a given location is erroneously denounced as 'damaged'.

Using the values of the thresholds defined for the undamaged state, the structural health monitoring can be carried out by comparing at each location the value of the interpolation error with the value of the threshold in the same direction.

2.5. *Numerical model of the building*

At the time being, only responses recorded during events that did not damage the factor building are available; hence, it is not possible to test the performance of the IDDM using real recorded responses. In order to check the performance of the damage localization algorithm, a numerical model of the factor building was developed using as a starting point the model used for the paper by Skolnik *et al*. [30]. The model was originally created on the basis of architectural and structural drawings and later updated applying an iterative sensitive-based method using the modal properties identified using responses to the Parkfield earthquake. In this model, the nonstructural elements are not explicitly modeled, and their effect on the global mass and stiffness is modeled by adding story stiffness and masses to the original model. These latter are calculated on the basis of the results of an identification procedures applied using responses recorded on the building during the Parkfield earthquake (see Reference [30] for more details on the model and on the identification procedure).

The main differences between the original model and the one used for this work concern the nonstructural elements that are explicitly modeled thus avoiding the addiction of dummy story mass and stiffness aimed to simulate their influence. BV and GCW on the building façades are modeled herein as shell elements with the characteristics reported in Table II.

The values of thickness and weight density were recovered from Reference [28], while the elastic moduli of BV and GCW were chosen in a range reasonable for the material and allowing to obtain a good match between the modal frequencies of the numerical model and values identified using data recorded during Parkfield earthquake of 28 September 2004 and reported in Table III.

Steel beams and columns are modeled with frame elements, assuming for the steel an elastic moduli of 2×10^8 MPa and a Poisson ratio of 0.3. Floors are modeled as rigid diaphragm with prevented in-plane relative displacements. The weight density of the floors is assumed equal to 20 kN/m^3 for stories

Table II. Characteristics of the exterior wall system.

	Brick veneer	Glass curtain walls
Thickness (cm)	3.8	0.64
Weight density (kN/m^3)	32	38
Elastic moduli (MPa)	2500	4350

Table III. Modal frequencies identified and calculated from the model.

Mode	Yorba Linda [31]	Encino [31]	Parkfield [28]	Parkfield [29]	F. E. Model
1°EW	0.51	0.50	0.47	0.47	0.47
1°NS	0.57	0.52	0.50	0.51	0.50
1°tors	0.70	0.70	0.68	0.68	0.70
2°EW	1.45 – 1.55	1.40 ÷ 1.65	1.49	1.48	1.48
2°NS	1.60 ÷ 1.75	1.50 ÷ 1.80	1.66	1.64	1.63
2°tors	/	/	2.36	2.37	2.33
3°EW	2.65 ÷ 2.85	2.45 ÷ 2.80	2.68	2.67	2.59
3°NS	2.75 ÷ 3.10	2.70 ÷ 3.05	2.86	2.88	2.73
3°tors	/	/	3.82	3.83	3.03

The character '/' means that no values were identified for the mode.

1–8 and equal to 30 kN/m^3 for stories 9–15. This distribution of masses, together with the introduction in the model of the stiffness of nonstructural elements, allows a close match between calculated and identified modal properties and is based on results presented in Reference [30]. Figure 10(b) and (c) reports two sections, along x and y directions, respectively, of the finite element model with the BV and the GCWs represented by the shell elements. In Table III, the first nine modal frequencies of the model are compared with the values of the same parameters identified by different research groups from responses recorded during several different small California earthquakes: 3 September 2002 Yorba Linda, 28 March 2003 Encino, and 28 September 2004 Parkfield.

The comparison between the values identified and calculated from the numerical model shows that there is a very good match for the first eight frequencies with maximum error lower than 5% for the Parkfield results. The error reaches 20% for the third torsional mode. This is probably due to the simplified distribution of floor masses, assumed as uniformly distributed in the model, but this approximation was considered acceptable for the model because it is has no influence on the results of the damage localization procedure herein presented.

To this respect, it is worth remarking that the numerical model was used just to simulate the behavior of a real building and to calculate the responses needed to feed the damage localization algorithm. In a real application of the damage localization procedure, one would use responses recorded on the real building without the need of a numerical model.

At the time being are available only responses recorded during events that did not damage the Factor Building hence it was not possible to test the performance of the IDDM using recorded data. For this reason, a numerical model was developed to simulate both the original configuration of the building and several different damage scenarios in order to calculate the responses needed to feed the damage localization algorithm.

The fit of the model to the experimental data was carried out to obtain a model ‘close’ to the real existing building, but the approximations related to the model does not influence at all the damage localization algorithm.

2.6. *Time history analysis of the building*

Linear time history analysis of the building has been performed to simulate the behavior of the building under vibrations before and after a damaging event, assuming that the structure can be modeled as a linear system before and after the onset of damage. The statistical variation of the interpolation error in the undamaged configuration of the numerical model has been assessed using responses of the

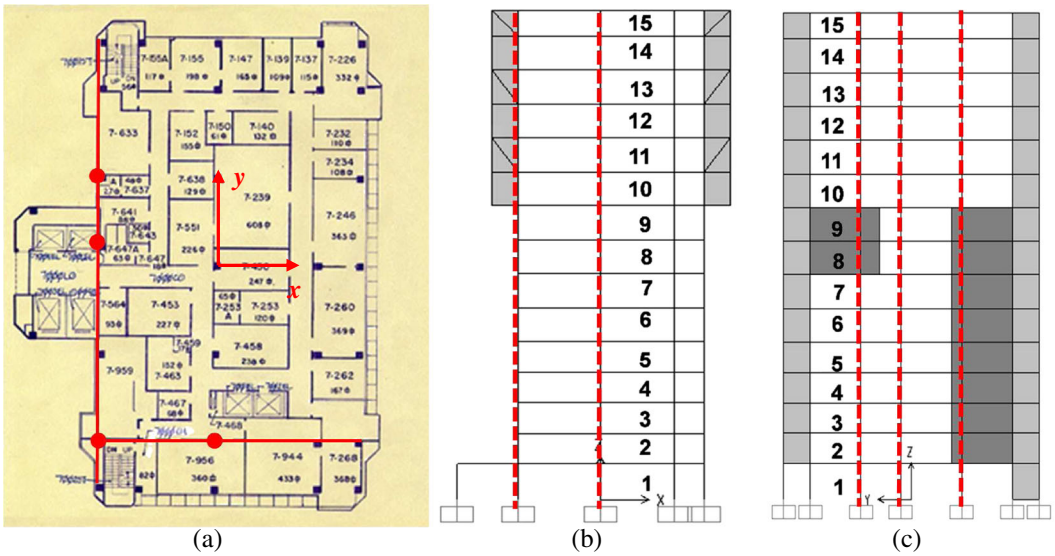

Figure 10. Location of the damaged columns (a) plan; (b) on the frame along x direction; and (c) on the frame along y direction.

model to the earthquakes reported in Table I. Damage has been simulated through pinned joints at columns end simulating a complete loss of flexural stiffness at these locations. This situation can be encountered if damage detection is performed using responses recorded before and after the possibly damaging event.

The base excitations in the x and y directions for the undamaged configurations were the same considered in Section 2.4 excepts event 273a that was used to excite the model in the damaged configurations. The values of the thresholds for the application of the IDDM have been recalculated for the model because the ambient conditions and all the other sources of variation of the interpolation error in the real structure were unknown, hence hardly reproducible in the model. Once the thresholds were calculated on the undamaged configuration, the performance of the IDDM was checked by simulating in the model several scenarios with damage localized at one or more stories and exciting the model with the base input recorded during the event 273a in Table I.

Several damage scenarios have been modeled assuming damage to two columns belonging to one frame in the x (or in the y) direction at one, two, three, or four stories. In Figure 10, a dot shows the plan locations of the damaged columns for the two frames in the x and in the y directions. Both single (damaged columns at one story) and multiple (damaged columns at two, three, or four stories) scenarios with increasing severity of damage (from one to seven damaged columns at the same story) have been considered. The names of the scenarios describe the location and severity of damage: For example, Dx_3_7_11_2c corresponds to a scenario with two damaged columns (2c) on the frame in x direction at the 3rd, 7th, and 11th stories. In order to give a quantitative description of the severity of the different damage scenarios considered herein, in Table IV are reported the values of the modal frequencies for each configuration. The first line of the table reports the values of modal frequencies for the original configurations (bolded values); in the following lines are reported the values of the modal frequencies only if it is different from the original ones: The character '/' means that no variation of the modal frequency occurs in the damaged configuration with respect to the original one. It is noted that the considered damage scenarios correspond to very small, almost negligible, variations of the modal frequencies. This is consistent with the small

Table IV. Modal frequencies for the original (bolded values) and the damaged scenarios.

	f_1	f_2	f_3	f_4	f_5	f_6	f_7	f_8	f_9
Undamaged	0.47	0.503	0.70	1.48	1.63	2.33	2.59	2.73	3.03
*Dx*_02_2*c*	/	/	/	/	/	2.32	2.58	2.72	/
*Dx*_04_2*c*	/	/	/	/	/	2.32	/	/	/
*Dx*_09_2*c*	/	/	/	/	/	2.32	2.58	/	/
*Dx*_04_12_2*c*	/	/	/	1.47	/	2.32	/	/	/
*Dx*_03_10_14_2*c*	/	/	/	1.47	/	2.32/	2.58	/	/
*Dx*_02_06_10_14_2*c*	/	/	/	1.47	/	2.31	2.57	2.72	/
*Dy*_03_2*c*	/	/	/	/	/	/	/	/	/
*Dy*_07_2*c*	/	/	/	/		/	/	/	/
*Dy*_13_2*c*	/	/	/	/		/	/	/	/
*Dy*_03_12_2*c*	/	/	/	/	1.62	/	/	/	/
*Dy*_03_07_11_2*c*	/	0.493	/	/		/	/	/	/
*Dy*_01_04_07_13_2*c*	/	0.495	/	/		2.31	/	2.70	/
*Dx*_06_1*c*	/	/	/	/		/	/	/	/
*Dx*_12_1*c*	/	/	/	/		/	/	/	/
*Dx*_08_1*c*	/	/	/	/		/	/	/	/
*Dy*_07_1*c*	/	/	/	/		/	/	/	/
*Dy*_07_3*c*	/	0.499	/	/		/	/	2.71	/
*Dy*_07_4*c*	/	0.497	/	/		2.32	/	2.71	/
*Dy*_07_5*c*	/	0.495	/	/		/	/	2.70	/
*Dy*_07_6*c*	/	0.495	/	/		/	/	2.69	/
*Dy*_07_7*c*	/	0.494	/	/		/	/	2.69	/
*Dy*_03_07_11_3*c*	/	0.493	/	/	1.62	2.31	/	2.71	/
*Dy*_03_07_11_5*c*	/	0.488	/	/	1.60	2.30	2.58	2.69	/
*Dy*_03_07_11_7*c*	/	0.484	/	1.47	1.60	2.30	2.58	2.67	/

The character '/' means that no change with respect to the original value occurs.

number of damaged element (maximum three columns per story) with respect to the total number of column of one story (about 40 columns). Notwithstanding the small amount of damage, the following results will show that, for the ideal case of responses not affected by noise, the IDDM is able to locate damage in almost all cases. Of course, in a real-world application where noise in recorded data plays an important role, the reliability of the IDDM in locating damage is lower and strictly depending on the quality or recorded responses.

3. RESULTS

Results for the different damage scenarios are reported in Figures 11–16 where the actual damage location is shown by the dashed blue area. Figures 11–14 refer to the ideal case of a noise to signal ratio of 0.1%, while Figures 15 and 16 describe the effect of noise on results.

The method has been applied using responses in the x direction for scenarios with damaged columns located in the frame along x (Dx) and responses in the y direction for scenarios with damaged columns in the frame along y (Dy).

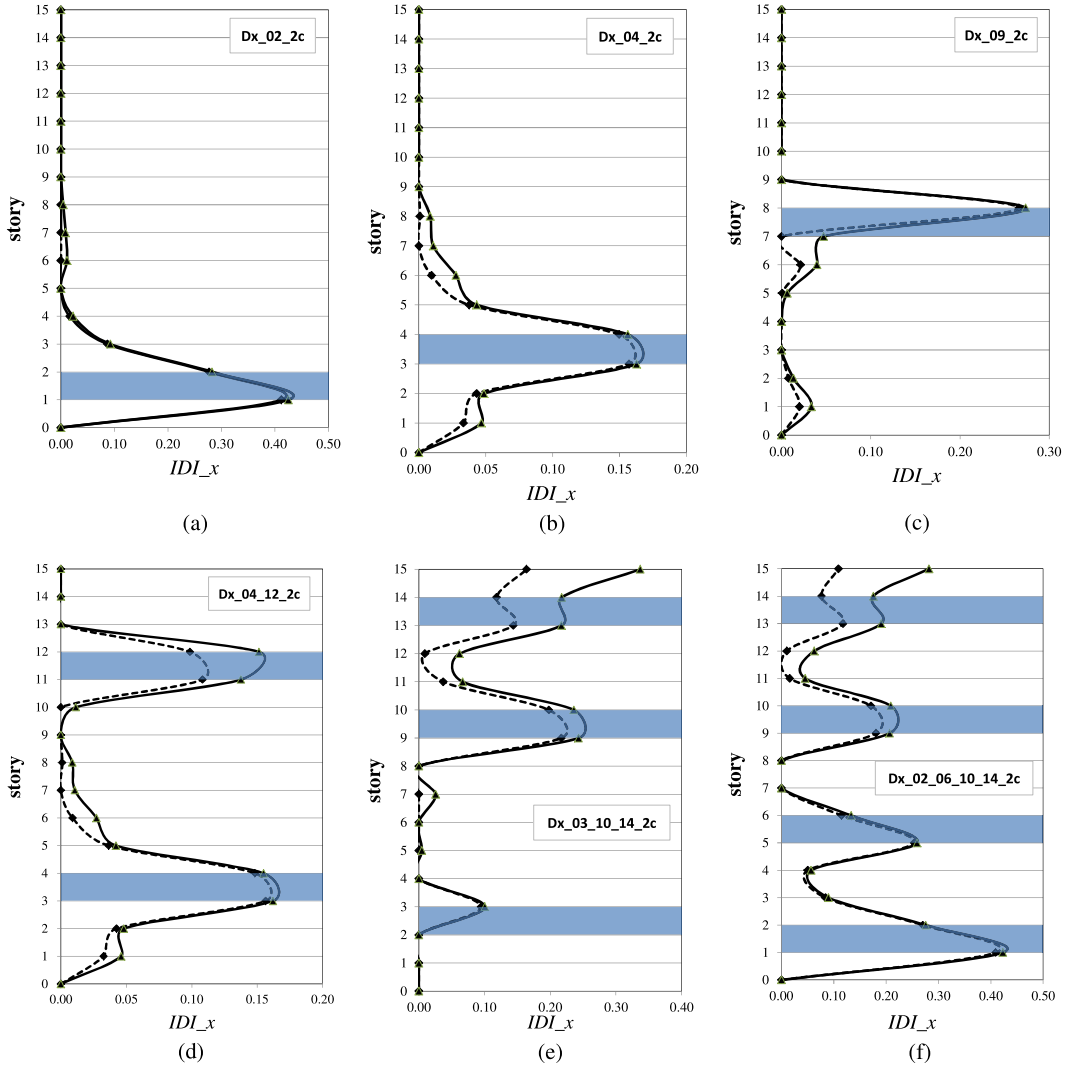

Figure 11. Results for damage at two columns located in one frame along the x direction at (a) the 2nd story; (b) the 4th story; (c) the 9th story; (d) the 4th and the 12th stories; (e) the 3rd, the 10th, and the 14th stories; (f) the 2nd, the 6th, the 10th, and the 14th stories (– – – – P_f=2%. -------- P_f=40%).

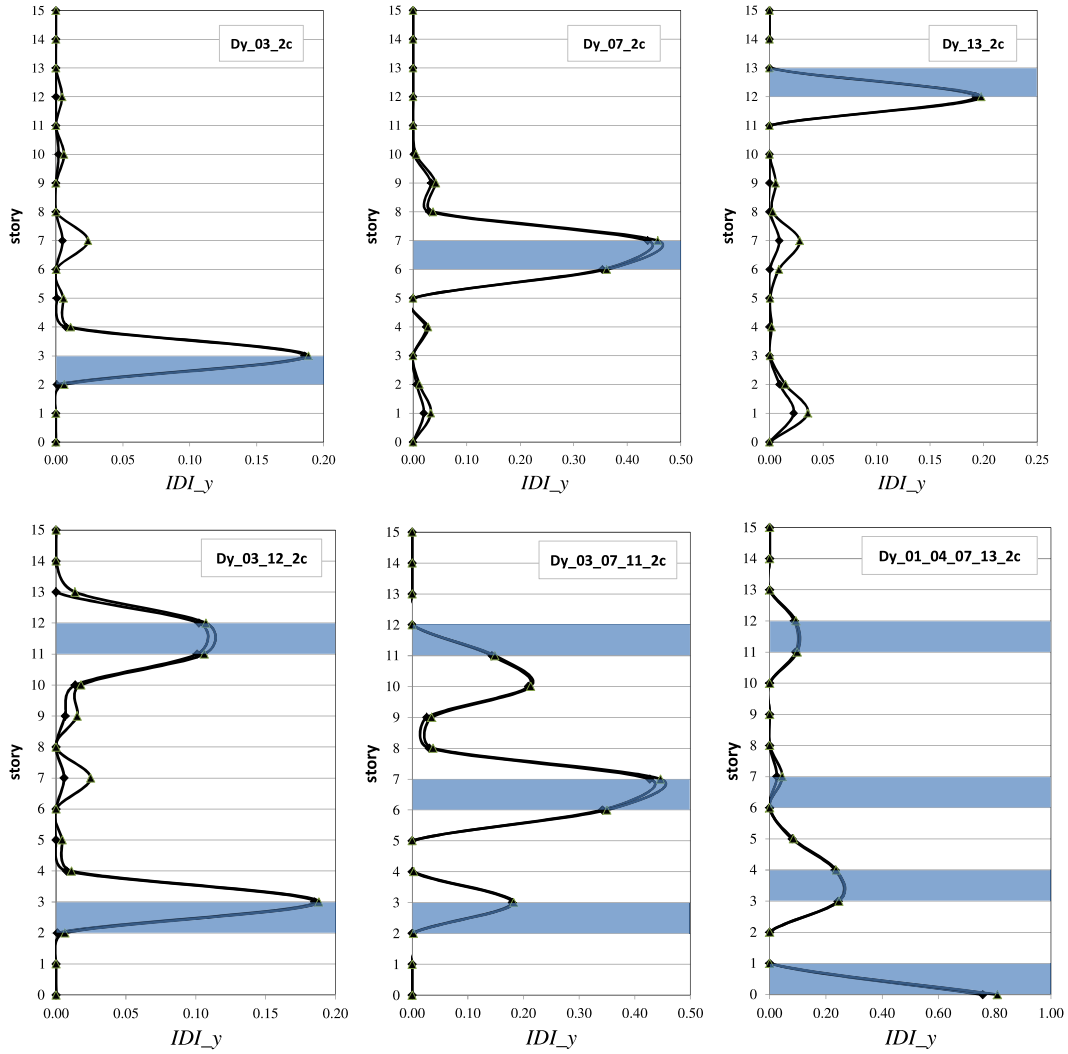

Figure 12. Results for damage at two columns located in one frame along the *y* direction at (a) the 3rd story; (b) the 7th story; (c) the 13th story; (d) the 3rd and the 12th stories; (e) the 3rd, the 7th, and the 11th stories; (f) the 1st, the 4th, the 7th, and the 13th stories (– – – – P_f=2%. -------- P_f=40%).

In order to study the influence of the value chosen for the probability of false alarm P_f, results in both *x* and *y* directions have been calculated assuming two different values of P_f. The two curves reported in Figures 15 and 16 correspond to the values P_f=40% and P_f=2%: The higher P_f, the lower the threshold $E_T(z)$, the higher the value of IDI (Equation (9)).

In the following, only results relevant to a number of the considered damage scenarios are reported, but the method is almost always successful in identifying the correct location of damage. Results show that in almost all cases, for two damaged columns per story, the method correctly detects the location of damage both for single and multiple damage location.

In a limited number of cases, the method is not able to identify the correct location of damage: This happens, for example, if damage is located at the 11th or at the 13th story in the *x* direction or at the 12th story in the *y* direction both for single and for multiple damage scenarios. The missing detection in these cases is likely to depend on the limited influence of the damaged elements on the story stiffness. For example, the stiffness at the 11th and at the 13th story in the *x* direction mainly depends on the two trusses (Figure 10(b)); hence. damage to the two columns induces a very small variation of the story stiffness that the method is unable to detect.

Missing detections have also been encountered for the majority of scenarios with one single damaged column at one story. The reduction of story stiffness was too low to be detected through

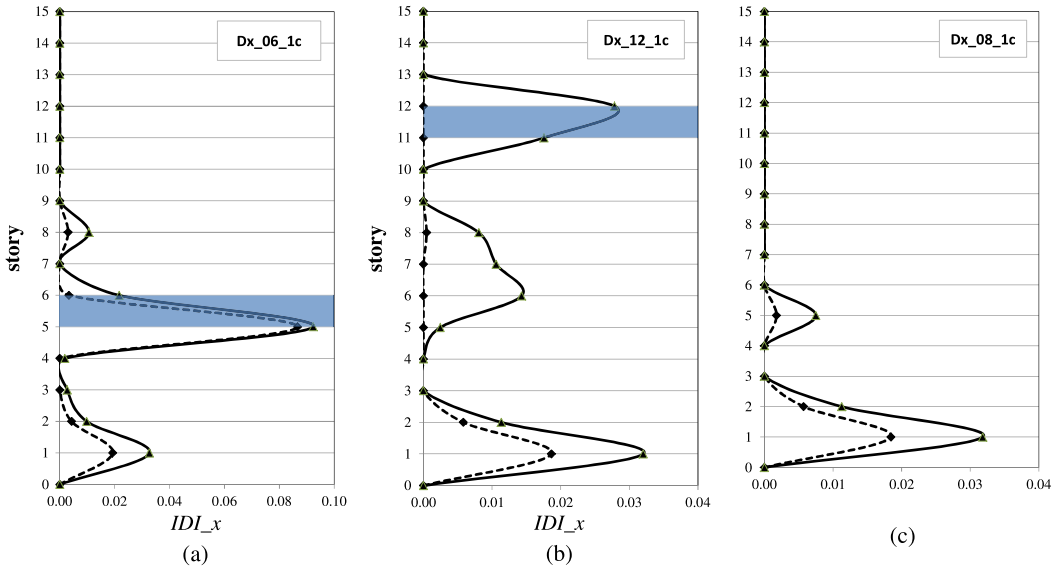

Figure 13. Results for damage at one column located in one frame along x direction at (a) the 6th story; (b) the 12th story; and (c) the 8th story (– – – – P_f=2%. -------- P_f=40%).

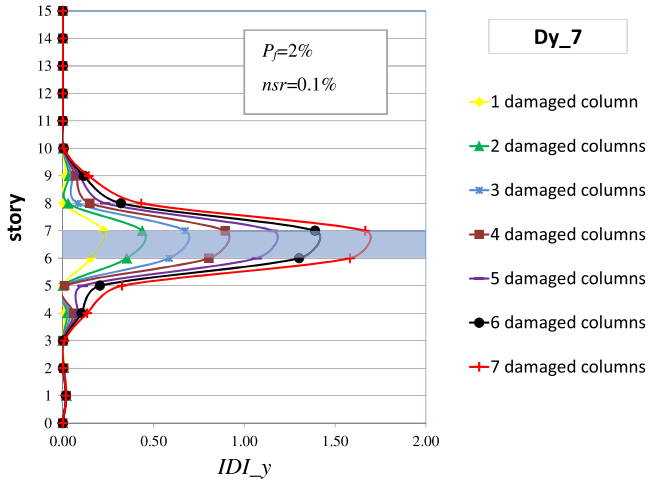

Figure 14. Increase of damage index with the severity of damage. Results for damage at an increasing number of columns in one frame along x direction at the seventh story. P_f=2%.

the interpolation method that becomes less reliable for very light damages: In some cases, the correct location of damage is detected as shown Figure 13(a); in other cases, in addition to the correct location of damage, the method erroneously detects damage at nondamaged locations (Figure 13(b)) making it difficult the correct identification of the actually damaged location. In other cases (Figure 13(c)), the damaged location is completely missed, and damage is erroneously detected only at an undamaged story.

All results previously reported were obtained using responses in the same direction of the damaged frame. The analysis of responses in the direction orthogonal to the damaged frame in many cases does not allow the localization of damage because of the small reduction of story stiffness in that direction. This remark can be useful to localize the direction of a damaged frame: If damage is detected only through the responses in one direction, then damage is likely to be located in one frame parallel to that direction.

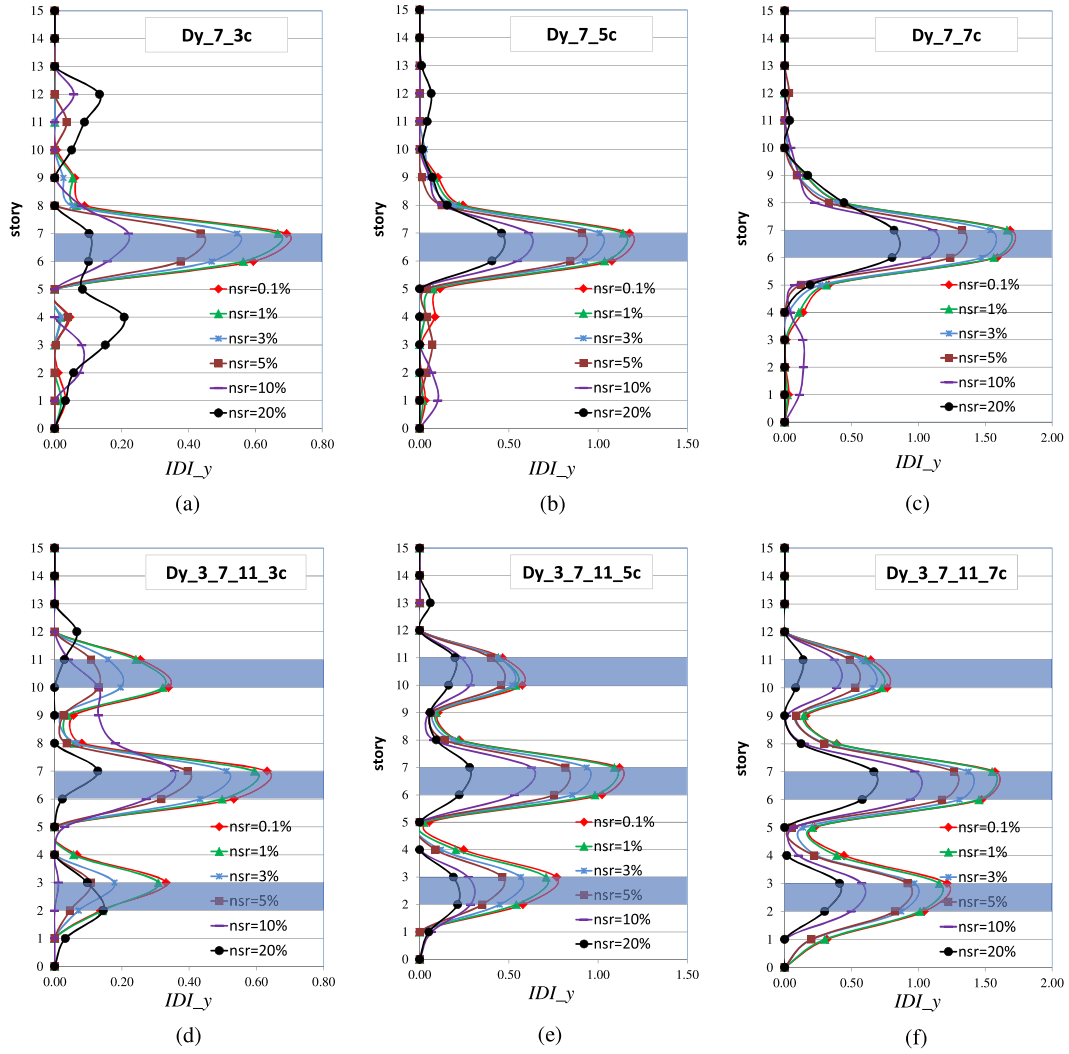

Figure 15. Influence of noise (from 0.1% to 20% of the signal-to-noise ratio) and severity of damage on the interpolation damage index (IDI) for false alarm probability $P_f = 40\%$. Results for damage in one frame along the y direction at (a) three columns at the 7th story; (b) five columns the 7th story; (c) seven columns the 7th story; (d) three columns at the 3rd, the 7th, and the 11th stories; (e) five columns at the 3rd, the 7th, and the 11th stories; and (f) seven columns at the 3rd, the 7th, and the 11th stories.

The value of the probability of false alarm for these ideal cases with a very low level of noise in responses has a limited influence the value of the damage index IDI.

At the increase of the severity of damage that is at the increase in the number of the damaged elements per story, the damage index IDI(z) also increases. In Figure 14, the values of the damage index are reported for several scenarios corresponding to an increasing number of damaged columns in one frame along y, at the 7th story.

At the moment, a relationship between the amount of damage and the value of the IDI has not yet been established; hence, it is not possible to recover the amount of damage from the value of the IDI.

The definition of such a relationship will be the object of following studies. It is apparent form the results reported herein that the value of the IDI depends both on the severity of damage and on the on the locations where the damage occurs: The same reduction of stiffness at two different stories corresponds to different values of the IDI as shown by the comparison between Figure 11(a)–(c) and Figure 12(a)–(c).

It is remarked that the previous results have been obtained considering signals free from noise that is quite unrealistic for real structures equipped with recording sensors. The previous results are just meant

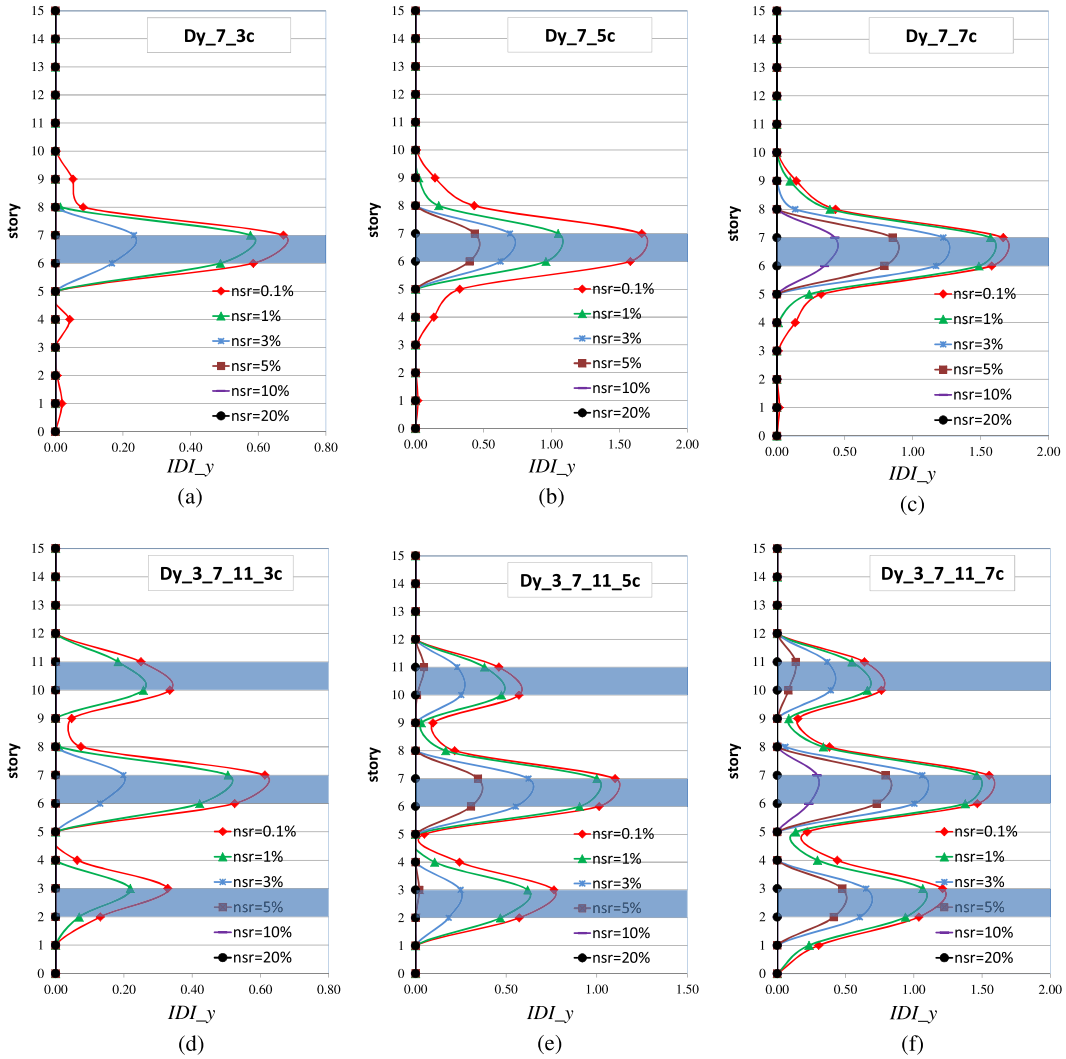

Figure 16. Influence of noise (from 0.1% to 20% of the signal-to-noise ratio) and severity of damage on the interpolation damage index (IDI) for false alarm probability $P_f = 2\%$. Results for damage in one frame along the y direction at (a) three columns at the 7th story; (b) five columns the 7th story; (c) seven columns the 7th story; (d) three columns at the 3rd, the 7th, and the 11th stories; (e) five columns at the 3rd, the 7th, and the 11th stories; and (f) seven columns at the 3rd, the 7th, and the 11th stories.

to show the capability of the method for the ideal case that is as much approximated as the quality of recording sensor increases. In the following, the effect of noise will be taken into account and investigated.

3.1. Influence of noise in recorded data

In order to study the influence of the quality of the available data on the reliability of the interpolation method, different levels of noise have been randomly added to the responses calculated by the numerical model.

Noise has been modeled as a Gaussian zero mean white noise vector: Several different simulations were carried out considering values of noise increasing from 1% to 20%. The percentage represents the ratio between the root mean square of added noise and the root mean square of the amplitude of the absolute acceleration. Results show that the reliability of the method depends on the relationship between the severity of damage, on the intensity of noise, and the value chosen for the threshold. In Figure 15 reports results for different intensity of noise and for damage of increasing severity (three,

five, or seven damaged columns) A rough estimate of the reduction of stiffness per story is given by the number of damaged columns with respect to the total number of columns at the story (38 columns): One damaged column corresponds approximately to a reduction of stiffness of 2.5%; seven damaged columns corresponds to about 18% story stiffness reduction. At the increase of damage, the value of the IDI increases, thus making easier the localization of the damaged story also for high levels of noise.

In the case of seven damaged columns for both one damaged location (Figure 15(c)) and four damaged locations (Figure 15(f)), the identification of the damaged location is very clear. For damage of low severity (three damaged columns, Figure 15(a)), the correct localization of damage is hampered by a number of false alarms that arise when the signal-to-noise ratio reaches values higher than 5%. Results reported in Figure 15 have been obtained assuming an accepted probability of false alarm equal to 40%.

In Figure 16 are reported the results for the same damage scenarios but assuming a lower value of $P_f = 2\%$.

Low values of P_f lead to very higher values of the threshold E_t, and this hampers in some cases the detection of lighter damages for medium to high levels of noise (Figure 16(a), (b), (d), and (e)). For high level of noise ($nsr = 20\%$), damage is never detected both for single and for multiple damage scenarios.

The comparison between Figures 15 and 16 shows that the capability of the method to correctly detect damaged locations depends on the value chosen for the threshold and on the level of noise: The higher the noise, the lower has to be chosen the threshold (hence, the higher has to be chosen P_f) in order to reduce the rate of missing alarms. On the other hand, a high value of P_f (low value of the threshold) limits the capability of the method to detect light damages because it implies increasing the rate of false alarms. As already underlined, being the choice of the threshold a trade-off between the two probabilities, a preliminary analysis must be carried out to carefully choose its value taking into account all the possible sources that influence results and the actual possibilities to keep the level of noise in recorded responses as low as possible. In any case, the acquisition of high quality signals with a low signal-to-noise ratio plays a key role in the increase of the reliability of results and must be a central issue for this, as well as for the majority of damage identification methods.

4. CONCLUSIONS

In this paper, the IDDM has been successfully proposed for the case of the UCLA factor building, a real densely instrumented multistory steel building. The method, on the basis of the investigation of statistically meaningful changes in the so-called interpolation error, enables to detect localized variations of stiffness using acceleration responses recorded on the building. The IDI is defined in terms of the exceedance of a threshold of the interpolation error corresponding to the rate of false alarms that, in the undamaged state of the building, is considered tolerable by the owner of the structure or by the responsible of the structural safety. The first step in the application of the IDI is the characterization of the statistical variation of the interpolation error in the undamaged state of the structure based on responses recorded on the structure during a period long enough. This first step has been carried out in this paper using responses recorded on the building during a number of small earthquakes that occurred throughout 2004. Next, in order to investigate to capability of the IDDM to detect and localize damage, a calibrated numerical model of the building has been built and used to simulate several damage scenarios. Results show that, even for the case of noisy data, this method allows a reliable detection of both single and multiple locations of damage, provided a sufficiently dense network of instruments is deployed. The capability of the method to locate damage is influenced by the level of noise and by the severity of damage: Medium to severe damages can be easily detected by the method also for medium to high level of noise in recorded signals; while in order to detect small reductions of stiffness, high quality signals must be recorded on the structure. The main advantage of the IDDM with respect to other methods of damage localization is that it does not require a numerical model of the structure and an intense data post-processing or user interaction. For these reasons, this method appears as a valid option for automated damage assessment, able to provide after a damaging event reliable information about the location of damage.

ACKNOWLEDGEMENTS

The author wish to thank the USGS ANSS program and the NSF Center for Embedded Networked Sensing at UCLA for the availability of data recorded on the factor building and Dr. Derek Skolnik for the availability of his numerical model of the factor building.

REFERENCES

1. Çelebi M, Sanli A, Sinclair M, Gallant S, Radulescu D. Real time seismic monitoring needs of a building owner and the solution–a cooperative effort. *Earthquake Spectra*, EERI 2004; **20**(2):333–346.
2. Sohn H, Farrar CR, Hemez FM, Shunk DD, Stinemates DW, Nadler BR. A review of structural health monitoring literature: 1996–2001. *Rep. No. LA-13976*-MS, Los Alamos National Laboratory, Los Alamos, N.M., 2003.
3. Fan W, Qiao P. Vibration-based damage identification methods: a review and comparative study. *Structural Health Monitoring* 2011; **10**(1):83–29.
4. Yan YJ, Cheng L, Wu ZY, Yam LH. Development in vibration-based structural damage detection technique. *Mechanical Systems and Signal Processing* 2007; **21**(5):2198–2211.
5. Friswell MI. Damage identification using inverse methods. *Philosophical Transactions of the Royal Society A* 2007; **365**:393–410.
6. Nakamura M, Masri SF, Chassiakos AG, Caughey TK. A method for non-parametric damage detection through the use of neural networks. *Earthquake Engineering and Structural Dynamics* 1998; **27**:997–1010.
7. Hung S-L, Kao CY. Structural damage detection using the optimal weights of the approximating artificial neural networks. *Earthquake Engineering and Structural Dynamics* 2002; **31**:217–234.
8. Farrar CR, Doebling SW. An overview of modal-based damage identification methods. *EUROMECH 365 International Workshop*: *DAMAS 97*, *Structural Damage Assessment Using Advanced Signal Processing Procedures*, Sheffield, U.K., 1997.
9. Capecchi D, Vestroni F. Monitoring of structural systems by using frequency data. *Earthquake Engineering and Structural Dynamics* 1999; **28**:447–461.
10. Pandey AK, Biswas M, Samman MM. Damage detection from changes in curvature mode shapes. *Journal of Sound and Vibration* 1991; **145**(2):321–332.
11. Kim JT, Stubbs N. Improved damage identification method based on modal information. *Journal of Sound and Vibration* 2002; **252**(2): 223–238.
12. Topole KG, Stubbs N. Non-destructive damage evaluation of a structure from limited modal parameters. *Earthquake Engineering and Structural Dynamics* 1995; **24**:1427–1436.
13. Poudel UP, Fu G, Ye J. Wavelet transformation of mode shape difference function for structural damage location identification. *Earthquake Engineering and Structural Dynamics* 2007; **36**:1089–1107.
14. Ho YK, Ewins DJ. On the structural damage identification with mode shapes. *Proc. of the European COST F3 Conference on Structural Identification and Structural Health Monitoring*. Madrid, Spain 2000, 677–686.
15. Xia Y, Hao H, Brownjohn JMW, Xia P-Q. Damage identification of structures with uncertain frequency and mode shape data. *Earthquake Engineering and Structural Dynamics* 2002; **31**:1053–1066.
16. Safak E. Detection of seismic damage in structures from continuous vibration records (invited paper), *Proceedings*, *9th International Conference on Structural Safety and Reliability* (*ICOSSAR*), Rome, Italy, June 19–23, 2005.
17. Wang Z, Lin RM, Lim MK. Structural damage detection using measured FRF data. *Computer Methods in Applied Mechanics and Engineering* 1997; **147**:187–197.
18. Xu ZD, Wu Z. Energy damage detection strategy based on acceleration responses for long-span bridge structures. *Engineering Structures* 2007; **29**:609–617.
19. Hsu T-Y, Loh C–H. A frequency response function change method for damage localization and quantification in a shear building under ground excitation. *Earthquake Engineering and Structural Dynamics* 2012; DOI: 10.1002/eqe.2235.
20. Sampaio RPC, Maia NMM, Silva JMM. Damage detection using the frequency response function curvature method. *Journal of Sound and Vibration* 1999; **226**(5):1029-1042.
21. Ratcliffe CP. Damage detection using a modified laplacian operator on mode shape data. *Journal of Sound and Vibration* 1997; **204**(3):505–517.
22. Limongelli MP. Frequency response function interpolation for damage detection under changing environment. *Mechanical Systems and Signal Processing* 2010; DOI: 10.1016/j.ymssp.2010.03.004.
23. Domaneschi M, Limongelli MP, Martinelli L. Damage detection in a suspension bridge model using the Interpolation Damage Detection Method. In *Bridge maintenance, safety, management, resilience and sustainability*, – Biondini, Frangopol (eds), Taylor & Francis Group: London, 2012. ISBN 978-0-415-62124-3.
24. Limongelli MP. The interpolation damage detection method for frames under seismic excitation. *Journal of Sound and Vibration* 2011; **330**:5474–5489.
25. Limongelli MP. Two dimensional damage localization using the interpolation method. *Submitted to DAMAS 2013*. *Dublin*, *July 8–10*, 2013.
26. Limongelli MP. Optimal location of sensors for reconstruction of seismic responses through spline function interpolation. *Earthquake Engineering and Structural Dynamics* 2003; **32**:1055–1074.
27. Nayeri RD, Masri SF, Ghanem R, Nigbor RL. A novel approach for the structural identification and monitoring of a full-scale 17-storey building based on ambient vibration measurements. *Smart Materials and Structures* 2008; **17**:1–19.

28. USGS. Earthquake hazard program. UCLA Factor Seismic Array. (Available from: http://factor.gps.caltech.edu/node/61.)
29. Hazra B, Narasimhan S. Wavelet-based blind identification of the UCLA factor building using ambient and earthquake responses. *Smart Materials and Structures* 2010; **19**:1–10.
30. Skolnik D, Ying L, Yu E, Wallace JW. Identification, model updating, and response prediction of an instrumented 15-storey steel frame building. *Earthquake Spectra* 2006; **22**(3):781–802.
31. Kohler MD, Davis PM, Safak E. Earthquake and ambient vibration monitoring of the steel-frame UCLA factor building, *Earthquake Spectra* 2005; **21**:715–736.